Environmental Science & Technology

Article

pubs.acs.org/est

Lumped Pathway Metabolic Model of Organic Carbon Accumulation and Mobilization by the Alga *Chlamydomonas reinhardtii*

Jeremy S. Guest,[†,∥] Mark C. M. van Loosdrecht,[‡] Steven J. Skerlos,[§] and Nancy G. Love*[,†]

[†]Department of Civil and Environmental Engineering and [§]Department of Mechanical Engineering, University of Michigan, Ann Arbor, Michigan 48109, United States

[‡]Department of Biotechnology, Delft University of Technology, 2628 CJ Delft, The Netherlands

Supporting Information

ABSTRACT: Phototrophic microorganisms have significant potential as bioenergy feedstocks, but the sustainability of large-scale cultivation will require the use of wastewater as a renewable resource. A key barrier to this advancement is a lack of bioprocess understanding that would enable the design and implementation of efficient and resilient mixed community, naturally lit cultivation systems. In this study, a lumped pathway metabolic model (denoted the phototrophic process model or PPM) was developed for mixed phototrophic communities subjected to day/night cycling. State variables included functional biomass (X_{CPO}), stored carbohydrates (X_{CH}), stored lipids (X_{LI}), nitrate (S_{NO}), phosphate (S_P), and others. PPM metabolic reactions and stoichiometry were based on *Chlamydomonas reinhardtii*, but experiments for model calibration and validation were performed in flat panel photobioreactors (PBRs) originally inoculated with biomass from a phototrophic system at a wastewater treatment plant. PBRs were operated continuously as cyclostats to poise cells for intrinsic kinetic parameter estimation in batch studies, which included nutrient-available conditions in light and dark as well as nitrogen-starved and phosphorus-starved conditions in light. The model was calibrated and validated and was shown to be a reasonable predictor of growth, lipid and carbohydrate storage, and lipid and carbohydrate mobilization by a mixed microbial community.

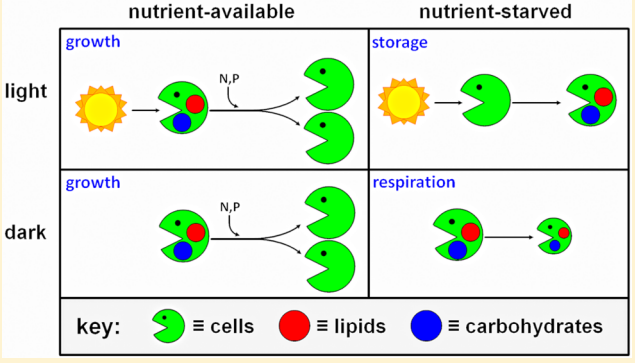

INTRODUCTION

Phototrophic microorganisms have distinct advantages over terrestrial bioenergy feedstocks including higher photosynthetic efficiencies, higher biomass productivity per land area, and the ability to be cultivated on nonarable land.[1] However, reliance on freshwater and synthetic fertilizers for biomass cultivation presents a significant challenge for large-scale biofuel production.[2] Recent studies have concluded the use of wastewater or wastewater treatment plant (WWTP) effluent may drastically decrease life cycle environmental impacts of cultivation[3] and could reduce the final cost of biodiesel by 50%.[4] The DOE National Algal Biofuels Technology Roadmap puts it simply: "Inevitably, wastewater treatment and recycling must be incorporated with algae biofuel production."[5]

In addition to the challenge of gaining access to wastewater resources,[6] a key barrier to the successful use of wastewater is a lack of efficient and resilient cultivation processes. To date, much of the research on cultivation has focused on biomass productivity and lipid content (as % of dry weight) in batch studies.[7] However, growth rate and cell composition (including stored lipids and carbohydrates) may be highly dynamic in a system with varying environmental conditions. Predicting the conditions that control the rate and extent to which organic carbon storage compounds are formed and degraded is key to the design of efficient and resilient bioprocesses, especially those that rely on natural light and have to cope with competition and predation in continuous systems.[8] As researchers and industry seek to advance bioenergy feedstocks, the ability to model biomass composition and growth enhances our understanding of process dynamics and may lead to the development of novel, mixed culture bioprocesses that reliably achieve target functions (e.g., lipid production).

A common approach to phototrophic process modeling has been the development of kinetic models stemming from experimental observations of cells and storage products (e.g., ref 9). This approach has advantages in terms of accessibility for designers and applicability to many species but limits one's ability to gain fundamental insight into the underlying factors influencing population dynamics and process performance in mixed microbial communities. More recently, molecular tools have enabled the construction of metabolic network models that explicitly model the rates of individual enzymatic processes and their impact on storage compounds. Published network models

Received: December 5, 2012
Revised: February 27, 2013
Accepted: March 1, 2013
Published: March 1, 2013

include hundreds of reactions and metabolites and have been used to evaluate metabolic engineering approaches in silico[10] and elucidate factors that influence biomass yields.[11,12] Although network models provide valuable insight into metabolic processes, they are computationally burdensome, may not be easily accessible to process engineers, and have a species specificity that may preclude their use in modeling mixed communities (e.g., those found in open cultivation systems). A hybrid approach, the development of lumped pathway metabolic models, combines the fundamental insight of metabolic network models with empirical process modeling practicality by representing the inter-related complex processes occurring simultaneously in the cell as a function of a single parameter upon which all are dependent.[13] This approach has been successful in improving mixed community bioprocess designs for wastewater treatment[14] by identifying selective pressures that provide competitive advantages for target functions (e.g., ref 15) and may offer similar advantages for phototrophic process design.

This paper presents a lumped pathway metabolic model for unicellular phototrophic microorganisms for nonaxenic bioprocess modeling. The phototrophic process model (PPM) was developed using the known metabolic pathways of *Chlamydomonas reinhardtii*, a model green alga which has been extensively studied, has well-characterized metabolic pathways, and is capable of both lipid and carbohydrate storage. *C. reinhardtii* is a member of the green algae, which are ubiquitous in diverse habitats and are the largest taxonomic group in which oleaginous phototrophs have been identified.[16] Consequently, it is expected to be a relevant model for phototrophs likely to proliferate in open cultivation systems, including those using wastewater or WWTP effluent as makeup water. To demonstrate the applicability of the PPM to a mixed community, experiments were performed in flat panel photobioreactors (PBRs) originally inoculated with biomass from a pilot-scale phototrophic system at a WWTP.

EXPERIMENTAL METHODS

Inocula and Growth Medium. Inocula were collected from an algaewheel pilot plant located after secondary treatment at the Hopewell Regional Wastewater Treatment Facility (City of Hopewell, Virginia). Mixed communities were maintained using a modified Allen's BG-11 medium[17] with silicate[18] and adjusted nitrogen and phosphorus concentrations. Medium was prepared with distilled water (ASTM type II) and the following nutrients ($mg \cdot L^{-1}$): $NaNO_3$ (750), K_2HPO_4 (78), $MgSO_4 \cdot 7H_2O$ (75), $CaCl_2$ (27), $Na_2SiO_3 \cdot 9H_2O$ (58), citric acid (6.0), ferric ammonium citrate (6.0), $Na_2 \cdot EDTA \cdot 2H_2O$ (1.04), Na_2CO_3 (20), H_3BO_3 (2.86), $MnSO_4 \cdot H_2O$ (1.55), $ZnSO_4 \cdot 7H_2O$ (0.22), $Na_2MoO_4 \cdot 2H_2O$ (0.39), $CuCl_2 \cdot 2H_2O$ (0.054), and $CoCl_2 \cdot 6H_2O$ (0.040).

PBRs. Three flat-plate PBRs with internal dimensions of 487 mm × 258 mm × 30 mm (height × width × depth) were constructed from UV-stabilized acrylic and filled to 3.0 L. PBRs were operated as cyclostats subjected to a daily light/dark cycle (14:10 h) at a dilution rate of 0.41 ± 0.01 d^{-1}. Cyclostats are chemostats subjected to a repeatedly varying light or temperature regime where cells are in a dynamic equilibrium of balanced growth and are appropriately poised for the estimation of model parameters.[19] The system was vented with a fan to reduce heat buildup, and reactors were mixed by continuous air sparging at 0.2–0.3 $L_{air} \cdot L_{reactor}^{-1} \cdot min^{-1}$. pH was maintained below 7.55 (typical pH was 7.35–7.55) using pH controllers operating solenoid valves delivering 99% CO_2 gas. Light was provided from both sides by a total of 16 fluorescent bulbs (Maxum 5000 48 in. F40-T12 MB, Full Spectrum Solutions; Jackson, MI), resulting in a surface irradiance of 400 ± 18 $\mu E \cdot m^{-2} \cdot s^{-1}$ PAR (photosynthetically active radiation, 400–700 nm) on each side, as measured by a quantum meter (Apogee MQ-303; Logan, UT) from the interior of each reactor. Average irradiance within each reactor was calculated using eq 1 (derived from the Beer–Lambert law, as in ref 20):

$$I_{avg} = 2 \cdot I_0 \cdot \frac{1}{b_{reactor}} (1 - e^{-a_C \cdot X_{VSS} \cdot b_{reactor}}) \cdot \frac{1}{a_C \cdot X_{VSS}} \quad (1)$$

Total and Volatile Suspended Solids (TSS, VSS). TSS (dry solids concentration) were determined by filtration through prerinsed, precombusted, preweighed glass fiber filters with 0.7 μm pore size (Whatman GF/F, item no. 0987472, Fisher Scientific; Pittsburgh, PA).[21] Filters were dried at 105 °C for at least 1 h and desiccated for a minimum of 30 min prior to weighing for TSS, followed by combustion in a muffle furnace at 550 °C for 20 min and at least 30 min of desiccation prior to weighing to determine VSS (i.e., ash free dry weight).

Proteins. Protein concentration was measured using the microbicinchoninic acid (micro BCA) method (item no. 23235, Thermo Scientific; Rockford, IL) modified with an alkaline digestion step.[22] Cells were resuspended in 1 N NaOH, incubated at 100 °C for 20 min, cooled to room temperature, and diluted 1:20 (sample volume/final volume) prior to the addition of micro BCA reagents. Absorbance was read on a microplate reader in triplicate wells at 562 nm. Bovine serum albumin (BSA) standards were treated identically to samples.

Lipids. Lipids were measured as fatty acid methyl esters (FAMEs) using the method of Levine and colleagues[23] with modifications. Briefly, samples with known VSS were pelleted in duplicate glass tubes, dried at 65 °C for 16–24 h, and stored at 4 °C. A 2 mL amount of acidified methanol was added to each glass tube, and the tubes were heated to 100 °C for 90 min with continual stirring, cooled to room temperature, and spiked with 1 mL of distilled and deionized (ASTM type I) water to stop the reaction. FAMEs were extracted into 4 mL of *n*-heptane containing 250 $mg \cdot L^{-1}$ of tricosanoic acid methyl ester (C23:0 FAME) as an internal standard (item no. 91478, Sigma–Aldrich; St. Louis, MO). FAMEs were identified and quantified by gas chromatography with flame ionization detection (GC-FID) with single injections (1 μL; 10:1 split ratio; 260 °C inlet temperature) onto a HP-InnoWax column (30 m × 0.32 mm × 0.25 μm; J&W 1909BD-113, Agilent Technologies; Santa Clara, CA) initially at 150 °C. After a 3 min hold, the temperature was ramped at 6 $°C \cdot min^{-1}$ to 260 °C and held for 9 min. Helium was the carrier gas at a constant flow rate of 1.0 $mL \cdot min^{-1}$. FID temperature was 300 °C. N_2 served as the makeup gas (25 $mL \cdot min^{-1}$). The relative standard deviation of the internal standard across all runs was 0.9%, and duplicate injections were shown to differ 1.5% on average for total lipids. Peaks were identified using an analytical standard (Supelco 37 Component FAME Mix, item no. 47885-U, Sigma–Aldrich) and quantified assuming the response ratio of each FAME (mg of (FAME)·$peak\ area^{-1}$) was equal to that of the internal standard.

Carbohydrates. Pelletable carbohydrates were measured using the method of Dubois[24] with dextrose as the standard and the following modifications. After the addition of 80% phenol and sulfuric acid, samples were digested at 90 °C for 5 min and cooled to room temperature for 30 min in the dark before reading the absorbance in triplicate microplate wells at 490 nm.

dx.doi.org/10.1021/es304980y | Environ. Sci. Technol. 2013, 47, 3258–3267

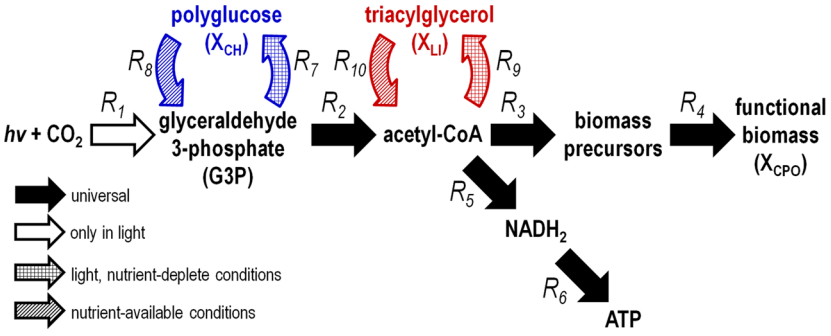

Figure 1. Schematic representation of the lumped pathway metabolic model for carbon-accumulating phototrophic organisms (X_{CPO}) capable of accumulating intracellular lipids (as triacylglycerol, X_{LI}) and carbohydrates (as polyglucose, X_{CH}). Although R_5 and R_6 are shown generating $NADH_2$ and ATP, respectively, $NADH_2$ and ATP are each produced and consumed in numerous reactions (see Table S1, Supporting Information).

The goal of this analysis was to quantify the changing concentrations of intracellular, carbohydrate-based storage polymers, which can be consistently measured with a short, heated acid digestion.[25] Longer digestions yield cell wall and other carbohydrates from the "functional" pool[25] and would have decreased the signal-to-noise ratio for this analysis, which was undesirable.

Nitrate and Soluble Phosphate. Samples were filtered through prerinsed 0.22 μm membranes (item no. GSWP 025 00, Fisher Scientific) prior to storage. Nitrate samples were stored in plastic tubes at −20 °C until analysis via triplicate injections using a DX-100 ion chromatograph (Dionex; Sunnyvale, CA) with an IonPac AS14 analytical column and eluent containing 3.5 mM Na_2CO_3 and 1.0 mM $NaHCO_3$. Soluble phosphorus samples were stored at 4 °C in acid-washed (HCl) glassware until analysis via the ascorbic acid method (method 4500-P-E[26]) modified for a microplate.

MODEL FORMULATION: METABOLISM

The developed lumped metabolic model (Figure 1) consists of 10 reactions (Reactions 1−10; R_1−R_{10}) provided in Table S1 (Supporting Information) and described in more detail in the subsections below. These reactions are based on the metabolic pathways of *C. reinhardtii*, noting many of the pathways are common among phototrophic microorganisms, and were used to solve for PPM stoichiometry.

Photosynthesis and Production of Acetyl-CoA. It is assumed the end products of photosynthesis (R_1) are glyceraldehyde-3-phosphate (G3P) and oxygen (O_2). Although cells may have auxiliary routes of electron transfer to match energy and reducing power conversion with metabolic needs,[27] it is assumed these auxiliary pathways are active at a rate designed to balance ATP/$NADPH_2$ production to meet the needs of carbon fixation.[28] G3P is converted to pyruvate via the Embden−Meyerhof−Parnas (EMP) pathway[10] and decarboxylated to form acetyl-CoA[11] (R_2).

Functional Biomass (X_{CPO}) Synthesis and Maintenance. The synthesis of functional biomass (anabolism) is modeled as two steps:[29] (i) the synthesis of functional biomass precursors (i.e., monomers; R_3); and (ii) the polymerization of those precursors into functional biomass (denoted X_{CPO} for carbon-accumulating phototrophs; R_4). The elemental composition of X_{CPO} and precursors is fixed as $CH_{1.8}O_{0.5}N_{0.2}$.[30] Carbon and nitrogen reduction is achieved via acetyl-CoA dissimilation to generate reducing equivalents (δ_x for carbon, δ_N for nitrogen),[31] and an ATP requirement (α_x) is included for polymerization of precursors to X_{CPO}.[32] The specific ATP consumption due to maintenance (m_{ATP}) was calculated based on experimental results.

Catabolism and Oxidative Phosphorylation. Catabolism of acetyl-CoA (R_5) occurs via the tricarboxylic acid (TCA) cycle.[10] ATP is also produced via oxidative phosphorylation (R_6) with the efficiency of this process expressed as the P/O ratio (δ_{PO}), which represents the moles of ATP produced per mole of $NADH_2$ oxidized.[13] Although the P/O ratio can vary with growth conditions,[33] the typical approach of maintaining a fixed ratio is used here.

Carbohydrate Storage and Mobilization. It is assumed carbohydrates are stored in the form of polyglucose, PG (X_{CH}; R_7), which is equivalent to starch or glycogen. G3P is converted to glucose 6-phosphate via gluconeogenesis,[11] requiring one ATP per molecule of glucose for polymerization. For the mobilization of X_{CH} (R_8), phosphorylated glucose monomers are removed from intracellular PG chains and converted to G3P via the EMP pathway.

Lipid Storage and Mobilization. Although cells may store lipids in numerous forms, for model construction, it is assumed fatty acids stored as neutral lipids are synthesized from acetyl-CoA to form palmitic acid (C16:0) and esterified to a glycerol molecule to form triacylglycerol, TAG (X_{LI}; R_9). G3P is assumed to be present in the cell during TAG synthesis and is the precursor for L-glycerol 3-phosphate. For the mobilization of X_{LI} (R_{10}), TAG is first hydrolyzed to glycerol and fatty acids by lipases. Glycerol is then phosphorylated to glycerol 3-phosphate, oxidized to dihydroxyacetone phosphate, and isomerized to G3P.[10] Palmitate requires one ATP for activation to palmitoyl-CoA[34] before degradation to acetyl-CoA.

Stoichiometry. Although not all reactions can be explicitly measured, internal reactions can be related to observable rates for system modeling.[13] First, linear equations for the rate of change of each component in the metabolic model were written for each of two cases: (i) nutrient-available (growth) conditions (Table S2, Supporting Information) and (ii) nutrient-deplete (non-growth) conditions (Table S3, Supporting Information). Each set of linear equations includes a reduction balance[30] and assumes no net accumulation of $NADH_2$, ATP, biomass precursors, acetyl-CoA, or G3P. Linear equations were solved using Mathematica 8.0.1.0 (Wolfram Research, Inc.; Champaign, IL) to determine stoichiometric relationships among *specific* rates (where "specific" rates are normalized to X_{CPO} concentration). Linear equation solutions and stoichiometric yields may be found in Tables S4 and S5 (Supporting Information), respectively.

dx.doi.org/10.1021/es304980y | *Environ. Sci. Technol.* 2013, 47, 3258−3267

Table 1. Kinetic Equations for PPM Transformation Processes

process [units]	rate expression
photoadaptation (P_1) [g of (Chl)·g of (C)$^{-1}$·h^{-1}]	$\left(\frac{0.2*\frac{I}{I_n}}{K_\gamma+\frac{I}{I_n}}\right)\cdot\left(0.01+0.03\frac{\ln\left(\frac{I}{I_n}+0.005\right)}{\ln(0.01)}-R\right)$
nitrate uptake (P_2) [mol of (N)·L^{-1}·h^{-1}]	$\hat{V}_{NO}\cdot\frac{S_{NO}}{K_{NO}+S_{NO}}\cdot X_{CPO}$
phosphorus uptake (P_3) [mol of (P)·L^{-1}·h^{-1}]	$\hat{V}_{P}\cdot\frac{S_{P}}{K_{P}+S_{P}}\cdot X_{CPO}$
photoautotrophic growth (P_4) [mol of (X_{CPO} as C)·L^{-1}·h^{-1}]	$\hat{\mu}\cdot\min\left[1-\left(\frac{Q_{N,min}}{Q_N}\right)^4,\ 1-\left(\frac{Q_{P,min}}{Q_P}\right)^4\right]\cdot f_I\cdot\left(1-\frac{\rho f_{CH}+f_{LI}\cdot\frac{Y_{CH}^{NR}}{Y_{LI}^{NR}}}{K_{STO}(1-f_I)+\rho f_{CH}+f_{LI}\cdot\frac{Y_{CH}^{NR}}{Y_{LI}^{NR}}}\right)\cdot X_{CPO}$
growth on stored carbohydrates (P_5) [mol of (X_{CPO} as C)·L^{-1}·h^{-1}]	$\hat{\mu}\cdot\min\left[1-\left(\frac{Q_{N,min}}{Q_N}\right)^4,\ 1-\left(\frac{Q_{P,min}}{Q_P}\right)^4\right]\cdot\max[f_I,\ \eta_{dark}]\cdot\left(\frac{\rho f_{CH}}{K_{STO}(1-f_I)+\rho f_{CH}+f_{LI}\cdot\frac{Y_{CH}^{NR}}{Y_{LI}^{NR}}}\right)\cdot X_{CPO}$
growth on stored lipids (P_6) [mol of (X_{CPO} as C)·L^{-1}·h^{-1}]	$\hat{\mu}\cdot\min\left[1-\left(\frac{Q_{N,min}}{Q_N}\right)^4,\ 1-\left(\frac{Q_{P,min}}{Q_P}\right)^4\right]\cdot\max[f_I,\ \eta_{dark}]\cdot\left(\frac{f_{LI}\cdot\frac{Y_{CH}^{NR}}{Y_{LI}^{NR}}}{K_{STO}(1-f_I)+\rho f_{CH}+f_{LI}\cdot\frac{Y_{CH}^{NR}}{Y_{LI}^{NR}}}\right)\cdot X_{CPO}$
stored carbohydrate degradation for maintenance (P_7) [mol of (X_{CH} as C)·L^{-1}·h^{-1}]	$m_{ATP}\cdot\left(\frac{Y_{CH}^{NR}}{Y_{ATP}}\right)\cdot\left(\frac{\rho f_{CH}}{K_{STO}+\rho f_{CH}+f_{LI}\cdot\frac{Y_{CH}^{NR}}{Y_{LI}^{NR}}}\right)\cdot X_{CPO}$
stored lipid degradation for maintenance (P_8) [mol of (X_{LI} as C)·L^{-1}·h^{-1}]	$m_{ATP}\cdot\left(\frac{Y_{LI}^{NR}}{Y_{ATP}}\right)\cdot\left(\frac{f_{LI}\cdot\frac{Y_{CH}^{NR}}{Y_{LI}^{NR}}}{K_{STO}+\rho f_{CH}+f_{LI}\cdot\frac{Y_{CH}^{NR}}{Y_{LI}^{NR}}}\right)\cdot X_{CPO}$
endogenous respiration (P_9) [mol of (X_{CPO} as C)·L^{-1}·h^{-1}]	$m_{ATP}\cdot\left(\frac{Y_{XCPO}}{Y_{ATP}}\right)\cdot\left(1-\frac{\rho f_{CH}+f_{LI}\cdot\frac{Y_{CH}^{NR}}{Y_{LI}^{NR}}}{K_{STO}+\rho f_{CH}+f_{LI}\cdot\frac{Y_{CH}^{NR}}{Y_{LI}^{NR}}}\right)\cdot X_{CPO}$
carbohydrate storage (P_{10}) [mol of (X_{CH} as C)·L^{-1}·h^{-1}]	$\hat{q}_{CH}\cdot\left(1-\left(\frac{f_{CH}}{f_{CH}^{max}}\right)^{\beta_1}\right)\cdot\max\left[\left(\frac{Q_{N,min}}{Q_N}\right)^4,\ \left(\frac{Q_{P,min}}{Q_P}\right)^4\right]\cdot f_I\cdot X_{CPO}$
lipid storage (P_{11}) [mol of (X_{LI} as C)·L^{-1}·h^{-1}]	$\hat{q}_{LI}\cdot\left(1-\left(\frac{f_{LI}}{f_{LI}^{max}}\right)^{\beta_2}\right)\cdot\left(\frac{Q_{N,min}}{Q_N}\right)^4\cdot f_I\cdot X_{CPO}$

MODEL FORMULATION: KINETICS AND IMPLEMENTATION

Nutrient Uptake. Nutrient (N and P) uptake follows Monod kinetics independent of internal stores of the respective nutrient,[35] and growth is limited by a single nutrient following Droop formulation (i.e., cell quota model).[36] The expression of relative pool size ($Q_{N,min}/Q_N$; $Q_{P,min}/Q_P$) is raised to the power of 4 based on experimental results that included observations of rapid transitions from growth to organic carbon storage. [Note: Empirical corrections to response functions (i.e., applying exponents to expressions that have a value between 0 and 1) are not without precedent in phytoplankton modeling.[37]]

Photosynthesis. The light dependency of photoautotrophic growth is approached as in the PHOBIA model[38] but with one modification, the introduction of K_γ. Briefly, light dependency is modeled using the Eilers–Peeters relationship,[39] and photoadaptation is addressed by including the chlorophyll/carbon ratio as a state variable (R).[40] For convenience, the adaptation of R is converted to a continuous equation through the addition of

dx.doi.org/10.1021/es304980y | Environ. Sci. Technol. 2013, 47, 3258−3267

K_γ (P_1, Table 1). The final expression quantifying the cell's maximum relative photosynthetic productivity (f_I, a unitless term with a value from 0 to 1) becomes

$$f_I = \frac{I}{I + I_n \cdot (0.25 - 5R) \cdot \left(\frac{I^2}{I_{opt}{}^2} - \frac{2 \cdot I}{I_{opt}} + 1 \right)} \quad (2)$$

Organic Carbon Storage and Mobilization. Consistent with the literature and experimentation, lipid and carbohydrate storage occur when growth is arrested due to N starvation and carbohydrate storage occurs when growth is arrested due to P starvation.[41,42] As in the modeling of polyhydroxyalkanoate storage kinetics,[43] it is assumed cells accumulate carbohydrates and lipids at the greatest rates when none are within the cell and gradually decrease their accumulation rate as maximum storage capacity (f_{CH}^{max} and f_{LI}^{max}, respectfully) is approached. Stored substrate degradation is limited by cell quotas (Q_N, Q_P) or the relative fraction of stored substrate (f_{CH},f_{LI}). Growth of X_{CPO} is distributed across photoautotrophic (P_4) and heterotrophic (P_5, P_6) processes, with the relative fractions of each storage compound transformed to equivalent units using derived yields (Table S5, Supporting Information). The term ρ was added to account for the more rapid mobilization of X_{CH} relative to X_{LI}, and a reduction term (η_{dark}) was included in growth rate expressions to account for reduced growth in the dark.

Maintenance and Endogenous Respiration. Similar to the approach of Beeftink et al.,[44] maintenance ATP demand (m_{ATP}) is held constant and is met by the degradation of substrate (X_{CH} and X_{LI}) when available and supplemented with endogenous respiration as needed.

Normalization of X_{CPO}. X_{CPO} was assigned a constant relative composition, with protein as the normalizing factor and lipid and carbohydrate content specified by the minimum observed ratios of lipid/protein and carbohydrate/protein. Any measured lipid or carbohydrate in excess of these ratios was assumed to be X_{LI} or X_{CH}, respectively. VSS of X_{CPO} were estimated using the average observed ratio of protein to VSS not stemming from X_{LI} or X_{CH}. Minimum nutrient quotas were fixed by assuming X_{CPO} composition ($CH_{1.8}O_{0.5}N_{0.2}$) and a N/P molar ratio of 10:1.[30]

Model Structure. Following the format of existing wastewater process models,[45] the PPM is presented as a vector of transformation rate equations (Table 1) and a stoichiometric matrix (Table S6, Supporting Information). The state variables and transformation processes are characterized with indices i and j, respectively. The stoichiometric coefficients are presented in the stoichiometric matrix (v_{ji}), and transformation rate equations are presented as vector σ_j. Therefore, the rate of production of component i (in units of mass$_i$·length^{-3}·time^{-1}) is the sum of each stoichiometric coefficient in column i multiplied by each transformation rate j ($r_i = \sum v_{ji} \cdot \sigma_j$, over all processes j).

Model Calibration, Validation, and Sensitivity Analysis. For calibration of kinetic parameters, batch studies were run by stopping flow and altering the light/dark regime. Reactors were spiked with nitrogen (as $NaNO_3$), phosphorus (as K_2HPO_4), and/or micronutrients as needed to observe nutrient-available, N-limited, or P-limited conditions in both light and dark for extended periods of time (3−6 days). All light calibration studies used the same light intensity as cyclostat daytime operation. PBR 3 was used for model calibration and validation. PBRs 1 and 2 were operated under similar conditions to ensure all trends (e.g., X_{CH} mobilization in dark, nutrient-available conditions) were observed in at least two reactors. Fixed stoichiometric and kinetic parameters can be found in Table S7 (Supporting Information). The remaining parameters were calibrated by minimizing the total relative error between measured and modeled data, where relative error (RE) for a given compound (k) across the number of time points (N) was defined as follows:[43]

$$RE_k = \sum_{i=1}^{N} \left[\frac{n_k^{measured}(t_i) - n_k^{model}(t_i)}{n_k^{measured}(t_i)} \right]^2 \quad (3)$$

Model calibration was achieved using data (n) from three batch experiments (compounds, k, used for calibration are listed in parentheses and were weighted equally): (i) light, nutrient-available conditions for calibration of $\hat{V}_{NO}$ (S_{NO}), $\hat{V}_P$ (S_P), $\hat{\mu}$ (X_{CPO}), and ρ (f_{CH}, f_{LI}); (ii) light, N-deplete conditions for calibration of $\hat{q}_{CH}$, $\hat{q}_{LI}$, f_{CH}^{max}, f_{LI}^{max}, β_1, and β_2 (X_{CPO},f_{CH},f_{LI}), as well as m_{ATP} (X_{CPO}); (iii) dark, nutrient-available conditions for calibration of η_{dark} (f_{CH}, f_{LI}). Parameters were calibrated sequentially (rather than simultaneously) to mitigate the risk of overfitting. Initial cell quotas (Q_N; Q_P) were calibrated based on the maximum observed X_{CPO} concentration for each batch study. Calibration was achieved using the GRG Nonlinear solver tool in Microsoft Excel. Validity of the model was evaluated by operating PBR 3 in batch mode with a 14 h light period under reduced surface irradiance (150 ± 6 μE·m^{-2}·s^{-1} PAR) followed by a 10 h dark period. Soluble phosphorus was maintained in excess of 8 mg of (P)·L^{-1} with spikes of nitrate at the start of the light (30 mg of (N)·L^{-1}) and dark (>200 mg of (N)·L^{-1}) cycles. The sensitivity of model outputs (specifically X_{CPO}, f_{CH}, f_{LI}) to model parameters was evaluated by varying each calibrated parameter by ±10% and observing the ratio of the percent change in the output to the percent change in the parameter across the validation study.[46] It should be noted that parameter values presented in Table 2 were determined to enable the demonstration of the PPM and are not intended to be representative of all phototrophic bioprocesses. As more studies are performed and the PPM is applied to many more data sets, our knowledge of expected values will undoubtedly increase.

Table 2. Calibrated PPM Parameters

parameter	value	unit
$\hat{q}_{CH}$	0.026	mol of (X_{CH} as C)·mol of (X_{CPO} as C)$^{-1}$·h^{-1}
f_{CH}^{max}	0.86	mol of (X_{CH} as C)·mol of (X_{CPO} as C)$^{-1}$
β_1	2.9	unitless
$\hat{q}_{LI}$	0.014	mol of (X_{LI} as C)·mol of (X_{CPO} as C)$^{-1}$·h^{-1}
f_{LI}^{max}	1.2	mol of (X_{LI} as C)·mol of (X_{CPO} as C)$^{-1}$
β_2	3.5	unitless
$\hat{V}_{NO}$	25	mmol of (N)·mol of (X_{CPO} as C)$^{-1}$·h^{-1}
$\hat{V}_P$	0.73	mmol of (P)·mol of (X_{CPO} as C)$^{-1}$·h^{-1}
$\hat{\mu}$	0.082	h^{-1}
η_{dark}	0.70	unitless
ρ	1.2	unitless
m_{ATP}	0.044	mol of (ATP)·mol of (X_{CPO} as C)$^{-1}$·h^{-1}

RESULTS AND DISCUSSION

PBR Performance. PBRs were operated continuously as cyclostats for more than 6 months prior to batch experimentation and model calibration/validation. PBR phosphate concentrations during normal cyclostat operation were below the minimum reporting level of 0.05 mg of (P)·L^{-1}, and nitrate concentrations were greater than 10 mg of (N)·L^{-1}. VSS

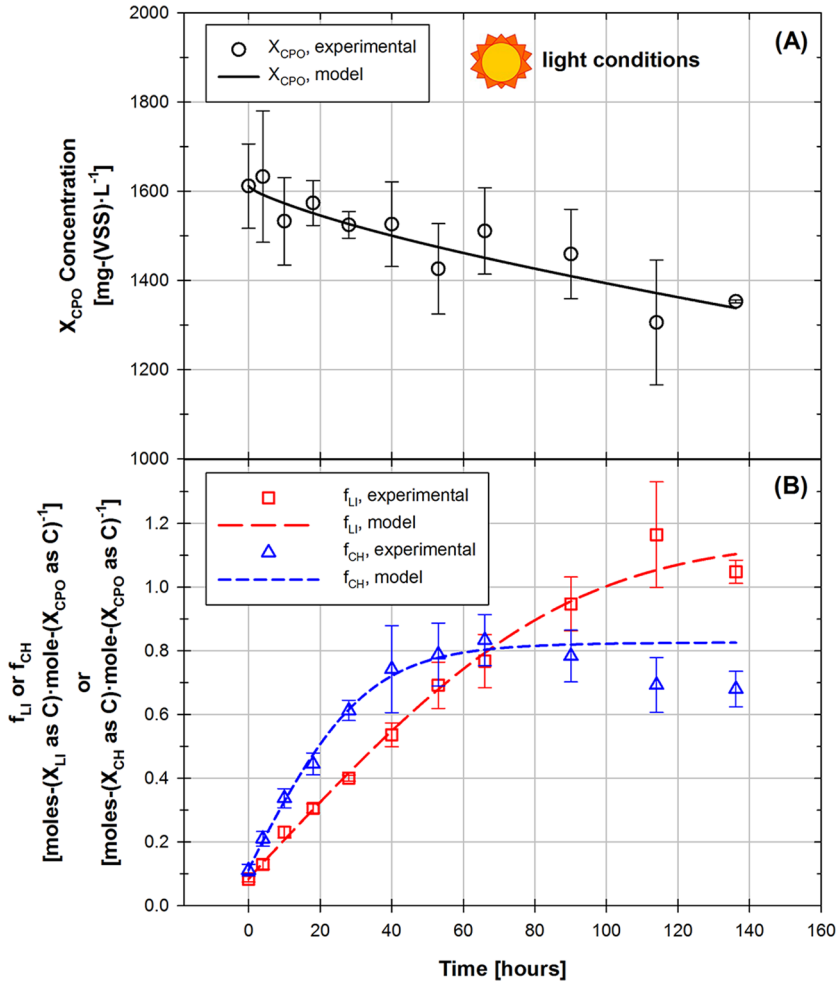

Figure 2. Experimental data (symbols) and calibrated model (lines) for (A) X_{CPO} and (B) f_{LI} and f_{CH} during the light, nitrogen-starved batch study on PBR 3. Data from the figures represents averages ± standard deviations of analytical replicates.

increased during the light period and decreased at night, with typical values from 1400 to 2200 mg of (VSS)·L^{-1} (VSS were 93 ± 3% of TSS) and an average ratio of 0.46 mg of (protein)·mg of (X_{CPO} as VSS)$^{-1}$. Although the absorption coefficient (a_c) changes with physiology, the measured value of 0.049 m^2·g of $(VSS)^{-1}$ was used to estimate average irradiance (I_{avg}). During normal cyclostat operation, I_{avg} was 250−360 $\mu E \cdot m^{-2} \cdot s^{-1}$, a reasonable target for naturally lit PBRs.[47] The minimum observed ratios of lipid/protein and carbohydrate/protein were 0.15 mg of (total lipids)·mg of $(protein)^{-1}$ and 0.19 mg of (carbohydrates)·mg of $(protein)^{-1}$, respectively. [Note: This ratio of carbohydrate/protein for total cell content is low because the carbohydrate analysis did not target all cell carbohydrates.] At the time of batch experimentation, microscopic examination revealed the communities in PBRs 1 and 3 were predominantly Chlorella-like while PBR 2 contained elevated concentrations of Scenedesmus-type and (possibly) cyanobacteria, all of which are relevant to wastewater treatment systems[7,48] and may be capable of organic carbon accumulation.[5] Although there will certainly be diversity of metabolisms within mixed communities that may cause slight differences in stoichiometry (e.g., a higher ratio of $ATP/NADPH_2$ production by cyanobacteria[28]), these may be partially accounted for via calibration of stoichiometric parameters. The processes and switching functions included in the final formulation of the PPM (e.g., carbohydrate accumulation during P starvation) were observed in all PBRs.

Lipid Accumulation. FAME analysis revealed stored lipids were predominantly long-chain fatty acids (C16 to C18; Figure S1, Supporting Information), a form of lipids highly relevant to downstream energy harvesting processes.[16] C16:0 (palmitic acid), in particular, was the primary C16 fatty acid (FA) stored across all three PBRs. C18 storage was spread among C18:0 (stearic acid), C18:1 (oleic and elaidic acids), C18:2 (linoleic and linolelaidic acids), and C18:3 (α-linolenic acid). Although individual forms of C18 FAs were observed at greater concentrations than C16:0 in some experiments, C16:0 was consistently stored and mobilized. For this reason, it is reasonable to represent X_{LI} as predominantly C16:0 molecules for model stoichiometry.

N starvation consistently resulted in lipid accumulation (as expected) while P starvation did not result in appreciable lipid accumulation in one of two PBR studies (PBR 2; data not shown). However, this result was not unexpected, as P starvation has been shown to have mixed impacts on lipid storage in microalgae.[42] Ultimately, a phosphorus switching function (based on relative pool size of phosphorus; $(Q_{P,min}/Q_P)^4$) could be added to P_{11} (as in P_{10}) if such behavior is observed in a given bioprocess. The PPM calibrated well to the trends in and magnitude of f_{LI} data with a R^2 of 0.98 across the calibration experiment (Figure 2B; calibrated parameters listed in Table 2). As a point of comparison, $\hat{q}_{LI}$ was equivalent to 0.0091 mg of (X_{LI})·mg of (X_{CPO} as VSS)$^{-1}$·h^{-1} that is similar to the maximum

dx.doi.org/10.1021/es304980y | Environ. Sci. Technol. 2013, 47, 3258−3267

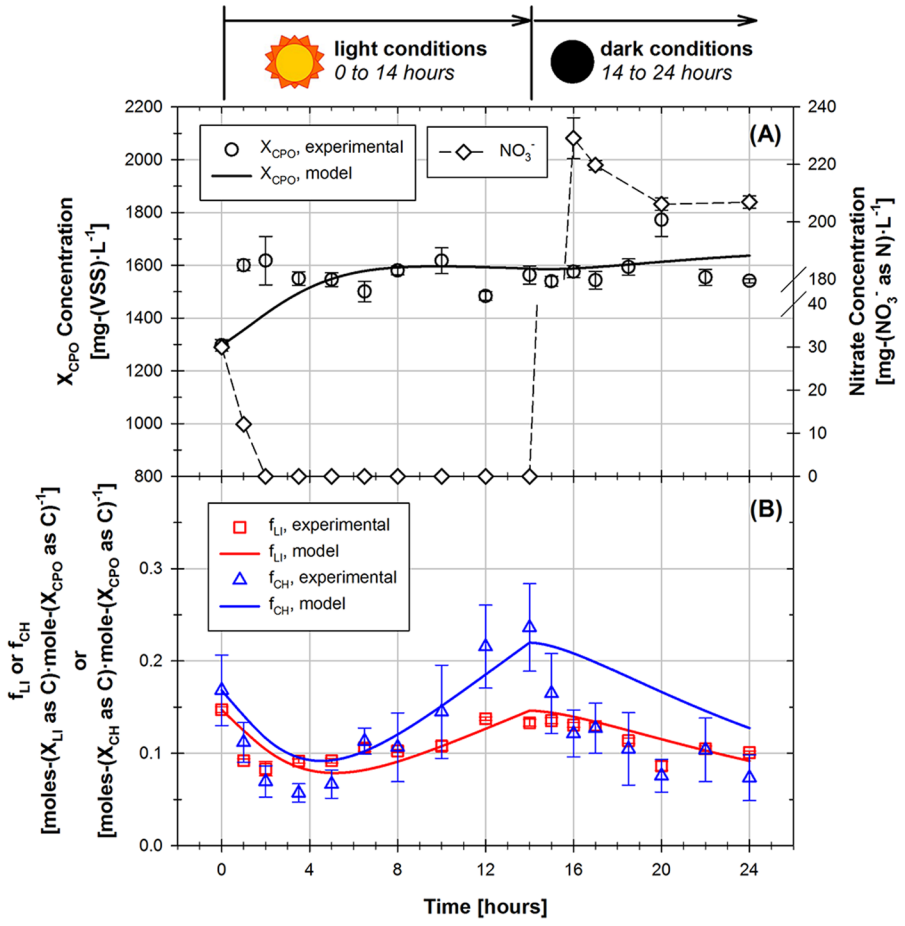

Figure 3. Validation study experimental data and modeling results for (A) X_{CPO} and (B) f_{LI} and f_{CH}. Measured nitrate values are presented in (A) to show nitrogen exhaustion, starvation, and reintroduction at 14 h (the start of the dark phase). Data from the figures represents averages ± standard deviations of analytical replicates.

rate of 0.012 mg of (neutral lipids)·mg of (functional biomass)$^{-1}$·h^{-1} that can be derived from work by Mairet et al.[9] if one assumes the same elemental composition of neutral lipids and functional biomass as assumed here for X_{LI} and X_{CPO}, respectively. The Mairet model was developed based on experimentation with *Isochrysis* aff. *galbana* under constant light and N-available, N-limited, and N-starved conditions[9] and offers a useful comparison for storage kinetics.

Carbohydrate Accumulation. Consistent with past observations,[41] N- or P-starvation resulted in X_{CH} accumulation. The PPM calibrated well to f_{CH} data (Figure 2B; R^2 of 0.91) with a maximum specific carbohydrate storage rate equivalent to 0.031 mg of (X_{CH})·mg of (X_{CPO} as VSS)$^{-1}$·h^{-1}. This storage rate is also similar to the maximum rate of 0.028 mg of (carbohydrate)·mg of (functional biomass)$^{-1}$·h^{-1} that can be derived from Mairet et al.[9] Although the maximum storage capacity of carbohydrates was 30% less than the maximum lipid storage (on a C basis), carbohydrate storage was more rapid with a maximum specific rate 80% faster than for lipids (Figure 2B).

Given that carbohydrates were also mobilized more quickly than lipids (discussed in more detail below), dynamic modeling for process design may be particularly important for bioethanol feedstock production. Phototrophic microorganisms have been shown to store polysaccharides in numerous forms including starch (e.g., green algae) and glycogen (e.g., cyanobacteria), which both have potential as bioethanol feedstocks.[49] These compounds are equivalent to PG in terms of energy and reducing power, thus enabling the use of the PPM for their explicit modeling. Phototrophs may also store polysaccharides in the form of chrysolaminarin (e.g., diatoms[50]), but modeling this compound would require alternate model formulation as it may degrade to free glucose[51] and require ATP for activation to glucose 6-phosphate.

Growth and Maintenance. The maximum specific growth rate ($\hat{\mu}$) was in the range of commonly reported values,[52] and the specific maintenance rate was equivalent to an endogenous respiration rate of 0.0053 h^{-1}. This maintenance rate was approximately 6.5% of the maximum specific growth rate, which is within the range of typical basal metabolism values reported for phototrophs (roughly 4−7%[52]) and could likely be reduced at higher growth rates.[12] The maximum specific rates of nitrate ($\hat{V}_{NO}$) and phosphate ($\hat{V}_P$) uptake calibrated well with R^2 values of 0.92 and 1.00, respectively. Once biomass with stored carbohydrates ($f_{CH} > 0$) was provided with nutrients, rapid mobilization of X_{CH} was consistently observed under both light and dark conditions. Lipid mobilization was also observed but at a reduced rate as compared to carbohydrates (captured by ρ). The PPM captured the general trends in growth and stored carbon mobilization well, which were consistent across all experiments including X_{CH} mobilization under dark conditions (Figure S2B, Supporting Information). However, the degree to which X_{LI} was mobilized in the dark varied across replicate reactors (Figure S2A, Supporting Information), an observation that warrants future research. Although the PPM was structured

dx.doi.org/10.1021/es304980y | Environ. Sci. Technol. 2013, 47, 3258−3267

such that X_{CH} and X_{LI} were mobilized simultaneously (based on observations here and in the literature[53]), some species may mobilize stored compounds sequentially.[54] An advantage of the PPM structure is that it can be easily modified for communities that predominantly utilize storage compounds sequentially by adding switching functions to P_S–P_8.

Validation and Future Model Advancements. The kinetic model structure was established using models and data from the literature as well as experimental data from PBRs. This model formulation was able to calibrate very well to PBR data (e.g., Figure 2) and captured the growth, storage, and mobilization trends of the low-light, one day validation study reasonably well (Figure 3; residuals plotted in Figures S3–S4, Supporting Information). Sensitivity analysis revealed predictions of X_{CPO} concentrations are far less sensitive to input parameters than f_{CH} or f_{LI}, and f_{CH} and f_{LI} are most dependent on $\hat{\mu}$, ρ, and their respective maximum specific rates of accumulation (Figure S5, Supporting Information). Model outputs were relatively insensitive to $\hat{V}_{NO}$, $\hat{V}_P$, β_1, β_2, f_{CH}^{max}, and f_{LI}^{max} but would be expected to demonstrate higher sensitivity to maximum carbon storage capacities for experiments that achieve higher levels of lipids or carbohydrate storage (i.e., f_{CH} approaches f_{CH}^{max}, f_{LI} approaches f_{LI}^{max}) as compared to the validation study. Future modeling efforts may focus greater attention on the short-term dynamics of transitions from light to dark or dark to light conditions. This may be achieved by reconciling traditional photosynthesis–irradiance relationships from limnology literature[39,40] with a mechanistic understanding of auxiliary electron transport pathways in microalgae[27] and observations of cell responses to rapidly fluctuating light conditions.[55] Such an understanding may enable engineers to design naturally lit bioprocesses to achieve target functions by explicitly integrating models of photosystem dynamics, hydrodynamics, and cell responses to environmental conditions (including temperature shifts,[56] light attenuation,[57] and higher light intensities) that may be observed in outdoor cultivation systems. Future work may also seek to better understand the extent of storage product mobilization under dark conditions (which varied for lipids across PBRs; Figure S2A, Supporting Information) and incorporate soluble organic carbon and other state variables from the activated sludge models (ASMs) into the PPM as a potential substrate for phototrophs:[58,59] an advancement that could enable the modeling of feedstock production processes using raw or primary-treated wastewaters as a source of water and nutrients. In fact, a significant advantage of the PPM structure is its similarity to traditional chemotrophic process models in wastewater treatment:[45] a characteristic that will enable its rapid integration into the existing wastewater modeling software (AQUASIM, GPS-X, BioWin, WEST, etc.) and knowledgebase, including established frameworks for model calibration to reduce the number of parameters adjusted in future modeling applications.[60]

There are distinct advantages to the use of a lumped metabolic model for process modeling, not the least of which is the mechanistic friction provided by elucidating stoichiometric relationships in terms of fundamental biochemical parameters (e.g., P/O ratio). By linking with complementary light attenuation and reactor models, the PPM may help elucidate nonaxenic bioprocess designs that will more efficiently and reliably achieve target functions (e.g., maximize lipid production) despite competition, predation, and the use of wastewater resources. As cultivation processes with wastewater are developed, however, it is vital that modeling be coupled with additional experimentation with laboratory- and pilot-scale systems to better understand the level of model complexity required to accurately predict long-term performance of mixed community phototrophic bioprocesses that recover resources from wastewater.

■ ASSOCIATED CONTENT

Supporting Information

Additional information as noted in the text. This material is available free of charge via the Internet at http://pubs.acs.org.

■ AUTHOR INFORMATION

Corresponding Author

*Phone: (734) 763-9664; fax: (734) 764-4292; e-mail: nglove@umich.edu.

Present Address

[‖]Jeremy S. Guest: Department of Civil and Environmental Engineering, University of Illinois at Urbana–Champaign, Urbana, Illinois 61801, United States.

Notes

The authors declare no competing financial interest.

■ ACKNOWLEDGMENTS

The authors would like to acknowledge financial support from the Graham Environmental Sustainability Institute and the Rackham Graduate School, both at the University of Michigan, for partial funding for the first author. The authors would also like to acknowledge Siddharth Dev and Harsha Hebbale for assistance in experimentation, Dr. Phillip Savage and Robert Levine for assistance with FAMEs analysis, Dr. Donald Scavia for helpful conversations related to model development, and Dr. J. Polle (Brooklyn College of CUNY) for help with microscopic analysis.

■ NOMENCLATURE

α_x	ATP required for polymerization of biomass precursors (monomers) to active biomass, mol of (ATP)·mol of $(X_{CPO}$ as C$)^{-1}$
β_1	power coefficient for carbohydrate storage inhibition, unitless
β_2	power coefficient for lipid storage inhibition, unitless
δ_N	CO_2 production from the catabolism of acetyl-CoA to generate reducing power for NO_3^- reduction for assimilation, mol of (CO_2 as C)·mol of $(X_{CPO}$ as C$)^{-1}$
δ_{PO}	efficiency of oxidative phosphorylation (P/O ratio) in mitochondria, mol of (ATP)·mol of $(NADH_2)^{-1}$
δ_x	CO_2 production from the synthesis of 1 C-mole of biomass from acetyl-CoA, mol of (CO_2 as C)·mol of $(X_{CPO}$ as C$)^{-1}$
η_{dark}	dark growth reduction factor, unitless
$\hat{\mu}$	maximum specific growth rate, mol of (X_{CPO} C)·mol of $(X_{CPO}$ as C$)^{-1}$·h^{-1}
ρ	carbohydrate relative preference factor, unitless
a_c	PAR absorption coefficient on a VSS or TSS basis, m^2·g of (VSS or TSS)$^{-1}$
$b_{reactor}$	thickness of reactor along light path, m
f_I	irradiance response function, unitless
f_{CH}	ratio of stored carbohydrates to cells, mol of (X_{CH} as C)·mol of $(X_{CPO}$ as C$)^{-1}$
f_{LI}	ratio of stored lipids to cells, mol of (X_{LI} as C)·mol of $(X_{CPO}$ as C$)^{-1}$
I_{avg}	average PAR irradiance within the PBR, μE·m^{-2}·s^{-1}

I_n maximum incident PAR irradiance ("irradiance at noon"), $\mu E \cdot m^{-2} \cdot s^{-1}$
I_o PAR irradiance at the interior surface of the PBR wall, $\mu E \cdot m^{-2} \cdot s^{-1}$
I_{OPT} optimal irradiance, $\mu E \cdot m^{-2} \cdot s^{-1}$
K_{NO} nitrate (as nitrogen source) half saturation coefficient, mol of (N)$\cdot L^{-1}$
K_P phosphorus half saturation coefficient, mol of (P)$\cdot L^{-1}$
K_{STO} stored substrate saturation constant, mol of (X_{CH} as C)·mol of (X_{CPO} as C)$^{-1}$
K_γ photoadaptation coefficient, unitless
m_{ATP} specific maintenance rate, mol of (ATP)·mol of (X_{CPO} as C)$^{-1}\cdot h^{-1}$
$\hat{q}_{CH}$ maximum specific carbohydrate storage rate, mol of (X_{CH} as C)·mol of (X_{CPO} as C)$^{-1}\cdot h^{-1}$
$\hat{q}_{LI}$ maximum specific lipid storage rate, mol of (X_{LI} as C)·mol of (X_{CPO} as C)$^{-1}\cdot h^{-1}$
Q_N nitrogen quota, mol of (N)·mol of (X_{CPO} as C)$^{-1}$
Q_P phosophorus quota, mol of (P)·mol of (X_{CPO} as C)$^{-1}$
R chlorophyll/carbon ratio, g of (Chl a)·g of (C)$^{-1}$
S_{CO2} soluble carbon dioxide, mol of (C)$\cdot L^{-1}$
S_{NO} soluble nitrate, mol of (N)$\cdot L^{-1}$
S_{O2} dissolved oxygen, mol of (O_2)$\cdot L^{-1}$
S_P soluble phosphorus, mol of (P)$\cdot L^{-1}$
$\hat{V}_{NO}$ maximum specific nitrate uptake rate, mol of (N)·mol of (X_{CPO} as C)$^{-1}\cdot h^{-1}$
$\hat{V}_P$ maximum specific phosphate uptake rate, mol of (P)·mol of (X_{CPO} as C)$^{-1}\cdot h^{-1}$
X_{CPO} concentration of carbon-accumulating phototrophic organisms, mol of (X_{CPO} as C)$\cdot L^{-1}$
X_{CH} concentration of stored carbohydrates, mol of (X_{CH} as C)$\cdot L^{-1}$
X_{LI} concentration of stored lipids, mol of (X_{LI} as C)$\cdot L^{-1}$
X_N concentration of cell-associated nitrogen, mol of (N)$\cdot L^{-1}$
X_P concentration of cell-associated phosphorus, mol of (P)$\cdot L^{-1}$
X_{VSS} concentration of volatile suspended solids, mg of (VSS)$\cdot L^{-1}$
Y_{ATP} yield of ATP on CO_2 fixed to G3P, mol of (ATP)·mol of (CO_2 as C fixed to G3P)$^{-1}$
Y_{CH}^{NR} yield of PG on CO_2 fixed to G3P, mol of (PG as C)·mol of (CO_2 as C fixed to G3P)$^{-1}$
Y_{LI}^{NR} yield of TAG on CO_2 fixed to G3P, mol of (TAG as C)·mol of (CO_2 as C fixed to G3P)$^{-1}$
Y_{XCPO} yield of carbon-accumulating phototrophic organisms on CO_2 fixed to G3P, mol of (X_{CPO} as C)·mol of (CO_2 as C fixed to G3P)$^{-1}$

REFERENCES

(1) Dismukes, G. C.; Carrieri, D.; Bennette, N.; Ananyev, G. M.; Posewitz, M. C. Aquatic phototrophs: Efficient alternatives to land-based crops for biofuels. *Curr. Opin. Biotechnol.* **2008**, *19*, 235−240.

(2) Vasudevan, V.; Stratton, R. W.; Pearlson, M. N.; Jersey, G. R.; Beyene, A. G.; Weissman, J. C.; Rubino, M.; Hileman, J. I. Environmental performance of algal biofuel technology options. *Environ. Sci. Technol.* **2012**, *46* (4), 2451−2459.

(3) Clarens, A. F.; Resurreccion, E. P.; White, M. A.; Colosi, L. M. Environmental life cycle comparison of algae to other bioenergy feedstocks. *Environ. Sci. Technol.* **2010**, *44* (5), 1813−1819.

(4) Menetrez, M. Y. An overview of algae biofuel production and potential environmental impact. *Environ. Sci. Technol.* **2012**, *46* (13), 7073−7085.

(5) U.S. Department of Energy. *National Algal Biofuels Technology Roadmap*; U.S. DOE, Office of Energy Efficiency and Renewable Energy, Biomass Program: Washington, DC, 2010; www1.eere.energy.gov/biomass/pdfs/algal_biofuels_roadmap.pdf.

(6) Fortier, M. O. P.; Sturm, B. S. M. Geographic analysis of the feasibility of collocating algal biomass production with wastewater treatment plants. *Environ. Sci. Technol.* **2012**, *46* (20), 11426−11434.

(7) Pittman, J. K.; Dean, A. P.; Osundeko, O. The potential of sustainable algal biofuel production using wastewater resources. *Bioresour. Technol.* **2011**, *102* (1), 17−25.

(8) Bull, J. J.; Collins, S. Algae for biofuel: Will the evolution of weeds limit the enterprise. *Evolution* **2012**, *66* (9), 2983−2987.

(9) Mairet, F.; Bernard, O.; Masci, P.; Lacour, T.; Sciandra, A. Modelling neutral lipid production by the microalga *Isochrysis* aff. *galbana* under nitrogen limitation. *Bioresour. Technol.* **2011**, *102* (1), 142−149.

(10) Manichaikul, A.; Ghamsari, L.; Hom, E. F. Y.; Lin, C. W.; Murray, R. R.; Chang, R. L.; Balaji, S.; Hao, T.; Shen, Y.; Chavali, A. K.; Thiele, I.; Yang, X. P.; Fan, C. Y.; Mello, E.; Hill, D. E.; Vidal, M.; Salehi-Ashtiani, K.; Papin, J. A. Metabolic network analysis integrated with transcript verification for sequenced genomes. *Nat. Methods* **2009**, *6* (8), 589−592.

(11) Boyle, N. R.; Morgan, J. A. Flux balance analysis of primary metabolism in *Chlamydomonas reinhardtii*. *BMC Syst. Biol.* **2009**, 3.

(12) Kliphuis, A. M. J.; Klok, A. J.; Martens, D. E.; Lamers, P. P.; Janssen, M.; Wijffels, R. H. Metabolic modeling of *Chlamydomonas reinhardtii*: Energy requirements for photoautotrophic growth and maintenance. *J. Appl. Phycol.* **2012**, *24* (2), 253−266.

(13) Roels, J. A. *Energetics and Kinetics in Biotechnology*; Elsevier Biomedical Press BV: Amsterdam, The Netherlands, 1983; p 330.

(14) Daigger, G. T. A practitioners perspective on the uses and future developments for wastewater treatment modelling. *Water Sci. Technol.* **2011**, *63* (3), 516−526.

(15) Lopez-Vazquez, C. M.; Oehmen, A.; Hooijmans, C. M.; Brdjanovic, D.; Gijzen, H. J.; Yuan, Z. G.; van Loosdrecht, M. C. M. Modeling the PAO-GAO competition: Effects of carbon source, pH and temperature. *Water Res.* **2009**, *43* (2), 450−462.

(16) Hu, Q.; Sommerfeld, M.; Jarvis, E.; Ghirardi, M.; Posewitz, M.; Seibert, M.; Darzins, A. Microalgal triacylglycerols as feedstocks for biofuel production: Perspectives and advances. *Plant J.* **2008**, *54*, 621−639.

(17) Allen, M. M.; Stanier, R. Y. Growth and division of some unicellular blue-green algae. *J. Gen. Microbiol.* **1968**, *51*, 199−202.

(18) Allen, M. M. Simple conditions for growth of unicellular blue-green algae on plates. *J. Phycol.* **1968**, *4* (1), 1−4.

(19) MacIntyre, H. L.; Cullen, J. J. Using cultures to investigate the physiological ecology of microalgae. In *Algal Culturing Techniques*; Andersen, R. A., Ed.; Elsevier Academic Press: London, 2005.

(20) Barbosa, M. J.; Zijffers, J. W.; Nisworo, A.; Vaes, W.; van Schoonhoven, J.; Wijffels, R. H. Optimization of biomass, vitamins, and carotenoid yield on light energy in a flat-panel reactor using the A-stat technique. *Biotechnol. Bioeng.* **2005**, *89* (2), 233−242.

(21) Pruvost, J.; Van Vooren, G.; Cogne, G.; Legrand, J. Investigation of biomass and lipids production with *Neochloris oleoabundans* in photobioreactor. *Bioresour. Technol.* **2009**, *100* (23), 5988−5995.

(22) Lowry, O. H.; Rosebrough, N. J.; Farr, A. L.; Randall, R. J. Protein measurement with the folin phenol reagent. *J. Biol. Chem.* **1951**, *193* (1), 265−275.

(23) Levine, R. B.; Pinnarat, T.; Savage, P. E. Biodiesel production from wet algal biomass through in situ lipid hydrolysis and supercritical transesterification. *Energy Fuels* **2010**, *24*, 5235−5243.

(24) Dubois, M.; Gilles, K. A.; Hamilton, J. K.; Rebers, P. A.; Smith, F. Colorimetric method for determination of sugars and related substances. *Anal. Chem.* **1956**, *28* (3), 350−356.

(25) Granum, E.; Myklestad, S. M. A simple combined method for determination of β-1,3-glucan and cell wall polysaccharides in diatoms. *Hydrobiologia* **2002**, *477* (1−3), 155−161.

(26) APHA; AWWA; WEF. *Standard Methods for the Examination of Water and Wastewater*, 21st ed.; APHA, AWWA, WEF: Washington, DC, 2006.

(27) Peltier, G.; Tolleter, D.; Billon, E.; Cournac, L. Auxiliary electron transport pathways in chloroplasts of microalgae. *Photosynth. Res.* **2010**, *106* (1−2), 19−31.
(28) Alric, J. Cyclic electron flow around photosystem I in unicellular green algae. *Photosynth. Res.* **2010**, *106* (1−2), 47−56.
(29) van Aalst-van Leeuwen, M. A.; Pot, M. A.; van Loosdrecht, M. C. M.; Heijnen, J. J. Kinetic modeling of poly(β-hydroxybutyrate) production and consumption by *Paracoccus pantotrophus* under dynamic substrate supply. *Biotechnol. Bioeng.* **1997**, *55* (5), 773−782.
(30) Roels, J. A. Application of macroscopic principles to microbial metabolism. *Biotechnol. Bioeng.* **1980**, *22* (12), 2457−2514.
(31) Gommers, P. J. F.; Vanschie, B. J.; Vandijken, J. P.; Kuenen, J. G. Biochemical limits to microbial growth yields: An analysis of mixed substrate utilization. *Biotechnol. Bioeng.* **1988**, *32* (1), 86−94.
(32) Verduyn, C.; Stouthamer, A. H.; Scheffers, W. A.; Vandijken, J. P. A theoretical evaluation of growth yields of yeasts. *Antonie van Leeuwenhoek* **1991**, *59* (1), 49−63.
(33) Stouthamer, A. H. A theoretical study on the amount of ATP required for synthesis of microbial cell material. *Antonie van Leeuwenhoek* **1973**, *39* (3), 545−565.
(34) Nelson, D. L.; Cox, M. M. *Lehninger Principles of Biochemistry*, 4th ed.; W.H. Freeman: New York, 2004; pp 1−100.
(35) Turpin, D. H. Physiological mechanisms in phytoplankton resource competition. In *Growth and Reproductive Strategies of Freshwater Phytoplankton*; Sandgren, C. D., Ed.; Cambridge University Press: Cambridge, U.K. 1988; p 448.
(36) Droop, M. R. Vitamin B_{12} and marine ecology. IV. The kinetics of uptake, growth and inhibition in *Monochrysis lutheri*. *J. Mar. Biol. Assoc. U. K.* **1968**, *48* (3), 689−733.
(37) Flynn, K. J.; Fasham, M. J. R.; Hipkin, C. R. Modelling the interactions between ammonium and nitrate uptake in marine phytoplankton. *Philos. Trans. R. Soc., B* **1997**, *352* (1361), 1625−1645.
(38) Wolf, G.; Picioreanu, C.; van Loosdrecht, M. C. M. Kinetic modeling of phototrophic biofilms: The PHOBIA model. *Biotechnol. Bioeng.* **2007**, *97* (5), 1064−1079.
(39) Eilers, P. H. C.; Peeters, J. C. H. A model for the relationship between light intensity and the rate of photosynthesis in phytoplankton. *Ecol. Modell.* **1988**, *42* (3−4), 199−215.
(40) Duarte, P.; Ferreira, J. G. Dynamic modelling of photosynthesis in marine and estuarine ecosystems. *Environ. Model. Assess.* **1997**, *2* (1−2), 83−93.
(41) Ball, S. G.; Dirick, L.; Decq, A.; Martiat, J. C.; Matagne, R. F. Physiology of starch storage in the monocellular alga *Chlamydomonas reinhardtii*. *Plant Sci.* **1990**, *66* (1), 1−9.
(42) Guschina, I. A.; Harwood, J. L. Lipids and lipid metabolism in eukaryotic algae. *Prog. Lipid Res.* **2006**, *45*, 160−186.
(43) Jiang, Y.; Hebly, M.; Kleerebezem, R.; Muyzer, G.; van Loosdrecht, M. C. M. Metabolic modeling of mixed substrate uptake for polyhydroxyalkanoate (PHA) production. *Water Res.* **2011**, *45* (3), 1309−1321.
(44) Beeftink, H. H.; Vanderheijden, R. T. J. M.; Heijnen, J. J. Maintenance requirements: Energy supply from simultaneous endogenouos respiration and substrate consumption. *FEMS Microbiol. Ecol.* **1990**, *73* (3), 203−209.
(45) Henze, M.; Gujer, W.; Mino, T.; van Loosdrecht, M. *Activated Sludge Models ASM1, ASM2, ASM2d and ASM3*; International Water Association: London, 2000.
(46) Van Veldhuizen, H. M.; Van Loosdrecht, M. C. M.; Heijnen, J. J. Modelling biological phosphorus and nitrogen removal in a full scale activated sludge process. *Water Res.* **1999**, *33* (16), 3459−3468.
(47) Wijffels, R. H.; Barbosa, M. J. An outlook on microalgal biofuels. *Science* **2010**, *329* (5993), 796−799.
(48) Hoffmann, J. P. Wastewater treatment with suspended and nonsuspended algae. *J. Phycol.* **1998**, *34*, 757−763.
(49) John, R. P.; Anisha, G. S.; Nampoothiri, K. M.; Pandey, A. Micro and macroalgal biomass: A renewable source for bioethanol. *Bioresour. Technol.* **2011**, *102* (1), 186−193.
(50) Roessler, P. G. UDPglucose pyrophosphorylase activity in the diatom *Cyclotella cryptica* - pathway of chrysolaminarin biosynthesis. *J. Phycol.* **1987**, *23* (3), 494−498.
(51) Kroth, P. G.; Chiovitti, A.; Gruber, A.; Martin-Jezequel, V.; Mock, T.; Parker, M. S.; Stanley, M. S.; Kaplan, A.; Caron, L.; Weber, T.; Maheswari, U.; Armbrust, E. V.; Bowler, C. A model for carbohydrate metabolism in the diatom *Phaeodactylum tricornutum* deduced from comparative whole genome analysis. *PLoS One* **2008**, *3* (1), e1426.
(52) Zhao, J. Y.; Ramin, M.; Cheng, V.; Arhonditsis, G. B. Competition patterns among phytoplankton functional groups: How useful are the complex mathematical models. *Acta Oecol.* **2008**, *33* (3), 324−344.
(53) Lacour, T.; Sciandra, A.; Talec, A.; Mayzaud, P.; Bernard, O. Neutral lipid and carbohydrate productivities as a response to nitrogen status in *Isochrysis* sp. (T-Iso; Haptophyceae): starvation versus limitation. *J. Phycol.* **2012**, *43* (3), 647−656.
(54) Siaut, M.; Cuine, S.; Cagnon, C.; Fessler, B.; Nguyen, M.; Carrier, P.; Beyly, A.; Beisson, F.; Triantaphylides, C.; Li-Beisson, Y. H.; Peltier, G. Oil accumulation in the model green alga *Chlamydomonas reinhardtii*: characterization, variability between common laboratory strains and relationship with starch reserves. *BMC Biotechnol.* **2011**, *11*, 7.
(55) Vejrazka, C.; Janssen, M.; Streefland, M.; Wijffels, R. H. Photosynthetic efficiency of *Chlamydomonas reinhardtii* in flashing light. *Biotechnol. Bioeng.* **2011**, *108* (12), 2905−2913.
(56) Bechet, Q.; Shilton, A.; Park, J. B. K.; Craggs, R. J.; Guieysse, B. Universal temperature model for shallow algal ponds provides improved accuracy. *Environ. Sci. Technol.* **2011**, *45* (8), 3702−3709.
(57) Huesemann, M. H.; Van Wagenen, J.; Miller, T.; Chavis, A.; Hobbs, S.; Crowe, B. A screening model to predict microalgae biomass growth in photobioreactors and raceway ponds. *Biotechnol. Bioeng.* **2013**, in press.
(58) Perez-Garcia, O.; Escalante, F. M. E.; de-Bashan, L. E.; Bashan, Y. Heterotrophic cultures of microalgae: Metabolism and potential products. *Water Res.* **2011**, *45* (1), 11−36.
(59) Bordel, S.; Guieysse, B.; Munoz, R. Mechanistic model for the reclamation of industrial wastewaters using algal-bacterial photobioreactors. *Environ. Sci. Technol.* **2009**, *43* (9), 3200−3207.
(60) Sin, G.; Van Hulle, S. W. H.; De Pauw, D. J. W.; van Griensven, A.; Vanrolleghem, P. A. A critical comparison of systematic calibration protocols for activated sludge models: A SWOT analysis. *Water Res.* **2005**, *39* (12), 2459−2474.